Hydrodynamic Modeling of Heaving Systems for Wave Energy Conversion

Pedro Tomás Pestana Mendonça

Abstract: This work presents a detailed study of the hydrodynamics modeling of a set of three distinct wave energy converters (WECs) based on real existing heaving point absorbers. For each WEC it is developed a frequency domain model to assess its performance for any given sea state. The hydrodynamic parameters are computed by the software WAMIT having posteriorly the solution of the motion equations and power-take-off (PTO) optimization executed by a MatLab code specifically made to solve these problems. The WECs are chosen considering their different configurations and features, resulting in the study applicable to a wide range of different heaving systems. Comparison of the responses of each device in regular and irregular waves is performed and their performance, for a case study where wave climates at two sites in Madeira Archipelago are considered, is evaluated. Lastly, to gain insight into the uncertainties of WEC performance, several sensitivity tests are carried out with the respective results being discussed.

1. Introduction

From the 173000 TW of solar power reaching the Earth's atmosphere, 1200 TW is converted into kinetic energy in form of wind which acting on the ocean surface generates currents and powerful waves [1]. These waves can travel huge distances without significant losses of energy and with a power density much higher than solar or wind power. A wave carries both kinetic and gravitational potential energy where its total energy depends mainly on two parameters, the height H and the period T. The global power potential represented by waves that hit all coasts worldwide has been estimated to be in order of 1 TW where is possible to extract up to 25% of energy, revealing to be a reliable resource of energy [2]. Having these phenomena in mind, several inventors were inspired by the possibility of converting the wave energy into usable energy.

1.1. Historical Background

The first patent referring to a device capable of converting energy from the waves is dated from back 1799 when Monsieur Girard and his son designed a prototype to drive energy from wave motion into saws, mills and other heavy machinery [3].

In 1910, Bochaux-Praceique developed the first device design to convert the energy of the wave into electrical power to supply his house at Royan, Bordeaux. This system is considered the first oscillating water column ever built [4].

Through the years, many wave converters were studied, reaching more than one thousand patents by 1980 [5]. Due to the growth of interest in this energy source field, many conferences have been held, papers and reports published.

Yoshio Masuda (1925-2009), a former Japanese naval officer, is considered as the father of modern wave technology due to his extensive studies in this field since the 1940s. Among his work, he developed a navigation

buoy powered by wave energy. This buoy was equipped with an air turbine having, therefore, developed a floating oscillating water column (OWC) device [6].

Later, in 1976, Masuda contributed for the construction of a large barge, named Kaimei, moored in Japan. This vessel was equipped with several set up of OWCs and different air turbines aboard in order to test their performance off-shore. The results of the output energy, however, did not match the expectations [7].

After the oil crisis, in 1973, many research institutes and universities revealed a growing interest in wave energy. Many new government-funded R&D programs initiated in UK, Sweden and Norway and later in few other countries [8]. However, the investment in this technology revealed to be sensitive to the oil price. Therefore, during periods of lower oil prices, the investment in wave energy technology was also significantly reduced. More recently, following the Kyoto protocol, there is again a growing interest in renewable energies, as wave energy.

1.1. Classification of WECs

WECs can be classified according to their geometry, size, orientation and technology as point absorbers, terminators, attenuators, overtopping, oscillating water column (OWC).

1.1.1. Point Absorber

A much smaller device compared with the predominant wavelength is named point absorber. A point absorber either floats on the free surface or is placed on the seabed. They mainly absorb energy due to the relative motion of their own components. The motion is imposed by the wave action and converted by some sort of conversion mechanism (mechanical, hydraulic) in linear or rotational motion.

Typically, this type of devices own a narrow bandwidth since this characteristic is directly related to the size of the WEC when compared with the wavelength, thus its efficiency is only significant in a short range of wave spectrum [9].

1.1.2. Attenuators and Terminators

Both terminators and attenuators are horizontally elongated floating WECs, with dimensions near to the wavelength, differing in their wave orientation. As previously mentioned, the bandwidth is greater with larger bodies and for this reason both terminators and attenuators are broadband WECs.

An attenuator is aligned parallel to the prevailing direction of wave propagation and therefore the wave travels along the WEC length. Usually, the attenuators ride the wave, meaning is body follows the free surface elevation being this device articulated in several points having the energy absorption located in those connections.

With an orientation perpendicular to the attenuator, the terminator is placed in order to face parallel to the wave crest. A terminator is a WEC that “terminates” the incoming wave. Due to its long extension, the wavefront acts as hitting a wall and the energy absorption is mainly from the wave energy is incident upon its length [10].

1.1.3. Overtopping

Overtopping devices captures the water that is close to the wave crest and introduce it, by over spilling, into a reservoir placed at a higher level than the average free-surface level. The potential energy of the stored water is converted into useful energy once it flows through low-head hydraulic turbines due to the pressure of its own weight [3].

1.1.4. Oscillating Water Column (OCW)

In general, these devices stand on the sea bottom or fixed to a rocky cliff. The OWC device comprises a partly submerged structure with an open below the water surface level and a chamber filled with air above it. The oscillating motion of the internal free surface produced by the incident waves forces the air to flow through a bi-directional turbine that drives an electrical generator. The bi-directional turbine makes use of airflow in both directions, thus this device can also generate power when the air passes through itself to refill the chamber.

To optimize an OWC the power take-off must be tuned in the wave periods and natural period of the water

column. Therefore, the design must be site-specific regarding the wave climate.

The shore line devices have the advantage of an easier installation and maintenance and absence of mooring and long underwater electrical cables. However, less energetic wave climate at the shoreline may be considered a preponderant disadvantage for its usage [11].

2. Governing Equations for Regular Waves

2.1. Two-body heaving converter

Typically, a point absorber is a floating axisymmetric two-body wave converter constrained to vertical oscillations imposed by the heave in deep water. The outer body 1 is a ring shape floating body. On the other hand, the inner body 2 is a long floating cylindrical body with a greater mass compared with the body 1. The gap between the two bodies is assumed small and the friction force neglected. The relative motion between the bodies drives the PTO usually placed on the top of the WEC.

Having x_1 and x_2 as the vertical coordinate of body 1 and 2 respectively, in absence of waves we have $x_1 = x_2 = 0$ where x_1 and x_2 positive axis is pointed upward. The mass of the PTO is neglected in comparison with m_1 and m_2 denoting the mass of body 1 and body 2 respectively.

Also, the force f_{PTO} of the PTO on the body 1 is considered as linear function of the relative displacement $x_1 - x_2$ and relative velocity $\dot{x}_1 - \dot{x}_2$. We have:

$$f_{PTO} = -K(x_1 - x_2) - C(\dot{x}_1 - \dot{x}_2) \quad (1)$$

where K and C are constants corresponding to the stiffness (spring) and damping of the PTO respectively and C is positive.

Applying the linear water wave theory, the equations for the dynamics and hydrodynamics of the two bodies may be written as:

$$m_1 \frac{d^2x_1}{dt^2} = f_{e,1} + f_{r,11} + f_{r,12} + f_{v,1} - g\rho S_1 x_1 + f_{PTO} \quad (2)$$

$$m_2 \frac{d^2x_2}{dt^2} = f_{e,2} + f_{r,22} + f_{r,21} + f_{v,2} - g\rho S_2 x_2 - f_{PTO} \quad (3)$$

where $f_{e,i}$ is the excitation force on body $i(i = 1,2)$ due to the incident wave, S_i is the water plane of the body $i(i = 1,2)$, $f_{r,ii}$ is the radiation force on body i due to its own motion, $f_{r,ij}$ is the radiation force on body i due to the motion of body j and $f_{v,i}$ is the viscous loss on body $i(i = 1,2)$.

In regular waves with radian frequency ω, amplitude A_w and linear PTO, we may write after the transient (when the initial conditions are vanished):

$$\{x_i, f_{e,i}, f_{r,ij}\} = Re[\{X_i, F_{e,i}, F_{r,ij}\}e^{i\omega t}] \quad (4)$$

where $X_i, F_{e,i}, F_{r,ij}(i, j = 1,2)$ are complex amplitudes and $Re[\,]$ their respective real part.

The radiation force $F_{r,ij}$ may be decomposed in:

$$F_{r,ij} = (\omega^2 A_{ij} - i\omega B_{ij})X_j \;\; (i, j = 1,2) \quad (5)$$

where A_{ij} is a real coefficient referring to the added mass and B_{ij} a real coefficient referring to the radiation damping. These coefficients depend on the wave frequency ω and on the geometry of the two-body systems.

The viscous resistance is given by:

$$f_{v,i} = -i\omega D_i X_i \quad (6)$$

where D_i is the viscous resistance coefficient. In the frequency domain, the dynamic equations can be expressed as:

$$\begin{aligned} &\{-\omega^2(m_1 + A_{11}) + i\omega(B_{11} + C + D_1) \\ &\quad + (g\rho S_1 + K)\}X_1 \\ &\quad + \{-\omega^2 A_{12} \\ &\quad + i\omega(B_{12} - C) - K\}X_2 \\ &\quad = F_{e,1} \end{aligned} \quad (7)$$

$$\{-\omega^2(m_2 + A_{22}) + i\omega(B_{22} + C + D_2) + (g\rho S_2 + K)\}X_2 + \{-\omega^2 A_{12} + i\omega(B_{12} - C) - K\}X_1 = F_{e,2} \quad (8)$$

The terms dependents of X_1 and X_2 were defined as:

$$\begin{cases} Z_1 = -\omega^2(m_1 + A_{11}) + i\omega(B_{11} + C + D_1) + (g\rho \\ Z_2 = -\omega^2 A_{12} + i\omega(B_{12} - C) - K \\ Z_3 = -\omega^2(m_2 + A_{22}) + i\omega(B_{22} + C + D_2) + (g\rho \\ Z_4 = -\omega^2 A_{12} + i\omega(B_{12} - C) - K \end{cases} \quad (9)$$

So, the equations 9 can be solved by the linear system:

$$\begin{bmatrix} Z_1 & Z_2 \\ Z_3 & Z_4 \end{bmatrix} \begin{bmatrix} X_1 \\ X_2 \end{bmatrix} = \begin{bmatrix} F_{e,1} \\ F_{e,2} \end{bmatrix} \quad (10)$$

And its solution is:

$$\begin{cases} X_1 = \dfrac{F_{e,1}Z_3 - F_{e,2}Z_2}{Z_2Z_4 - Z_1Z_3} \\ X_2 = \dfrac{F_{e,1}Z_4 - F_{e,2}Z_1}{Z_2Z_4 - Z_1Z_3} \end{cases} \quad (11)$$

The instantaneous power absorbed by the PTO is given by:

$$P(t) = -f_{PTO}\dot{X}_r = -f_{PTO}(\dot{x}_1 - \dot{x}_2) = C(\dot{x}_1 - \dot{x}_2)^2 + K(x_1 - x_2)(\dot{x}_1 - \dot{x}_2) \quad (12)$$

Therefore, in time average we have:

$$\bar{P} = \bar{P}_{PTO} = \frac{1}{2}C\omega^2|X_1 - X_2|^2 \quad (13)$$

2.2. Single-Body Heaving Converter

If we consider now the absence of the body 2 or in case of the one is fixed to the sea-bottom so $x_2 = 0$, the system is reduced to a single-body converter. In this situation, the absorbed power in not dependent of the relative motion between multiple bodies and therefore the equation 7 is reduced to:

$$\{-\omega^2(m_1 + A_{11}) + i\omega(B_{11} + C + D_1) + (g\rho S_1 + K)\}X_1 = F_{e,1} \quad (14)$$

The time average power is now:

$$\bar{P} = \frac{1}{2}C\omega^2|X_1|^2 \quad (15)$$

3. Response to Regular Waves

3.1. Heaving Systems

For this study, we have a pair of two-body heave converters and one submerged single-body heave converter. Each device was chosen due to its different design strategy.

The first WEC (WEC A) is modeled after the WaveBob™ (WaveBob Ltd, Ireland), featuring a positively buoyant floater and a streamlined reacting body with an integral water ballast tank (see Fig.1) [12], [13], [14].

Figure 1- WEC A.

The second (WEC B) is modeled after the PowerBuoy® (Ocean Power Technologies Inc, USA), featuring the same floater as WEC A but with a reacting body assembled with a large diameter heave plate (see Fig. 2) [15], [16] [17].

Figure 2- WEC B.

The third device (WEC C) is modeled after the Archimedes Wave Swing™ (Delft), featuring a submerged floater that reacts to a sea-bottom fixed structure (see Fig. 3) [18], [19].

Figure 3- WEC C.

3.2. Numerical Methods

In order to perform the numerical calculation, three distinct software were used such as: Rhinoceros for the 3D modelling and discretization of the systems meshes, WAMIT for the hydrodynamic coefficient computation and MatLab for the data processing and find the solution of the governing equations. Each surface of the models was divided into meshes of 20x10 sections, resulting into 1760, 1176 and 1080 panels for WEC A, WEC B and WEC C respectively. In the present study, the lower order method is used to discretize the body surface and is approximated with small quadrilateral panels. The velocity potential is assumed to be constant in each panel and thus the integral equations. The generated meshes were then exported directly to WAMIT as geometric data file. The Boundary Element Method (BEM) code WAMIT computed the inviscid hydrodynamic coefficients where both WEC A and WEC B were considered at infinite water depth and the WEC C bottom-mounted at 39.25m depth. The obtained data from WAMIT is then exported to a MatLab code. Once all hydrodynamic coefficients are known, the MatLab code computes the motion equation and consequently the power absorbed.

3.3. Hydrodynamic Coefficients

3.3.1. Added Mass

From Fig. 4 we can see that the added mass of the reacting body B is much greater than the remaining ones. Due to its heave plate, the WEC B owns a large surface opposing the motion direction, increasing greatly the added mass, hence its value is about 11 times greater than WEC B and 14 times greater than WEC C.

Considering the natural frequency is given by:

$$\omega_n = \sqrt{\frac{g\rho S_i}{m_i + A_{ii}}} \qquad (16)$$

The natural frequency ω_n is influenced by the added mass, hence the period of resonance is greater for the WEC B and out of the common range of wave periods. In the other hand, the lower added mass of bodies A and C is due to their streamlined design, behaving as "wave followers".

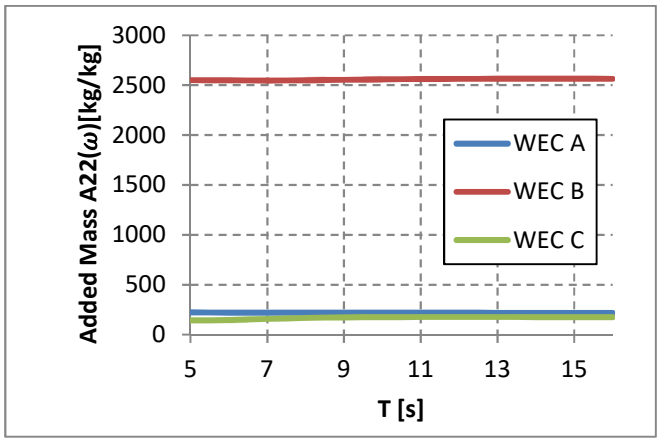

Figure 4- Added Mass.

3.3.2 Radiation Damping

In what concerns the radiation damping, the Fig. 5 shows the damping of reacting body is minimal and neglectable compared to bodies B and C. Due to its larger radius and proximity to the free surface, the floater of WEC C owns a larger radiation damping than the other systems while the radiation damping of the reacting body B is derived from its heave plate.

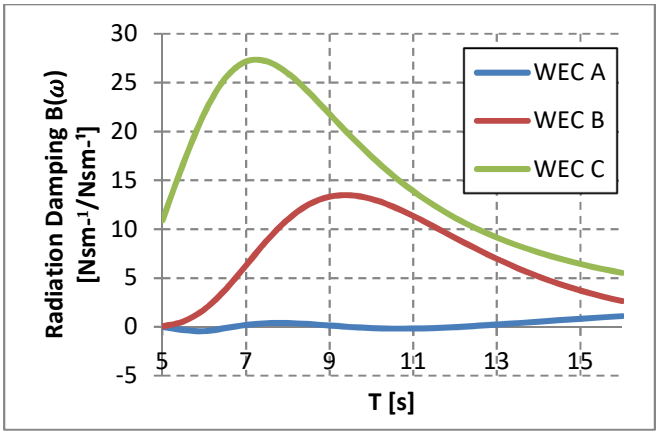

Figure 5- Radiation Damping.

3.3.3 Excitation Force

The Fig. 6 shows the excitation forces of the several oscillating bodies of each WEC where is included the floater of WEC A and WEC B since it corresponds to a significant amount of the total excitation forces of the systems.

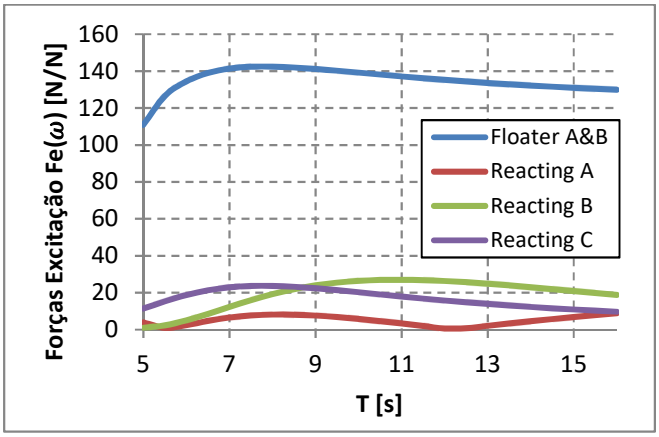

Figure 6- Excitation Forces.

3.3.4 Viscous Effects

Since BEM does not contemplate the viscous effects, an additional force concerning the viscous resistance must be included in the dynamic equations 7 and 8. The viscous resistance damping D is consider to be linear for mathematical convenience once it enables us to discuss the WECs in the frequency domain.

In this study, the viscous effect action was only considered on the reacting body (body $i = 2$) of WEC A and WEC B.

Is known the viscous resistance is given by:

$$f_v = \frac{1}{2}\rho A C_d U|U| \tag{17}$$

where A is the reference area, C_d the drag coefficient and U the fluid velocity. Now assuming this force as damping resistance represented by $D\dot{x}$ and assuming $U = \dot{x}$ we have:

$$D = -\frac{1}{2}\rho A C_d \dot{x} \tag{18}$$

Finally, from equation 4:

$$D = -\frac{1}{2}\rho A C_d \omega \, Re\{X e^{i\omega t}\} \tag{19}$$

Table 1 shows the drag coefficients considered for each WEC.

Table 1- List of Drag coefficients.

	C_d
WEC A	1.9
WEC B	2.8
WEC C	0.84

3.4. Power Capture

3.4.1. Power Maximization Strategies

In order to maximize the energy absorption and therefore yield a device economically viable, several PTO strategies may be adopted. Generally, the natural frequency of a point absorber system is lower than the incident waves, to settle the natural frequency of the system near to the wave frequency, a spring coefficient K is added to the PTO thus matching the resonance period of the system with the sea state T_p, yielding oscillations with higher amplitudes than water elevation. This PTO strategy is commonly named as *reactive.* If the PTO is equipped only a pure damping C it behaves as a passive dashpot and herein will be termed *passive*.

Another PTO strategy is the *latching.* This technique consists in a mechanism that holds the floater in a fixed position when it has reached the maximum amplitude and releases it after a certain interval (approximately a quarter of the period T_p).

3.4.2. Optimization

The optimization of the PTO permits to find the optimal values of damping C and spring K of the PTO so the power absorbed is maximum given the hydrodynamic parameters of the point absorber.

To compute the optimization, a Matlab iterative code was run. In this approach, the program varies the coefficients K and C in case of reactive PTO and C in case of passive PTO where the curve of power capture is plotted and the maximum value is obtained.

For an efficient tuning, the order of magnitude of K must match the mass of the bodies to keep the peak of resonance $0.5 < \omega_n < 1.4$ rad/s.

Results

The maximum power absorbed by each WEC is represented in Fig. 7, 8 and 9. The power obtained corresponds to the optimal values for each period i.e. a different value of C.

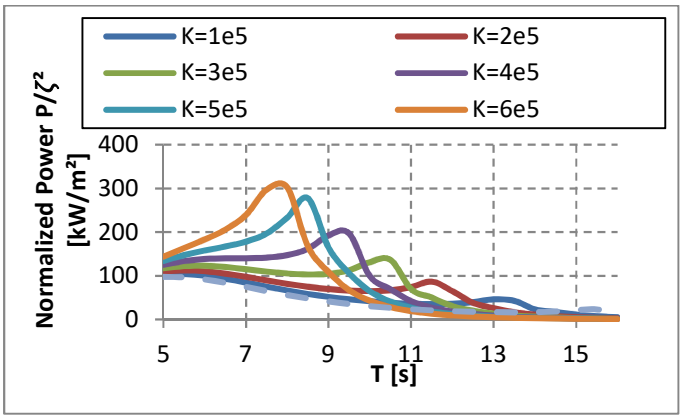

Figure 7- Optimized Power for WEC A.

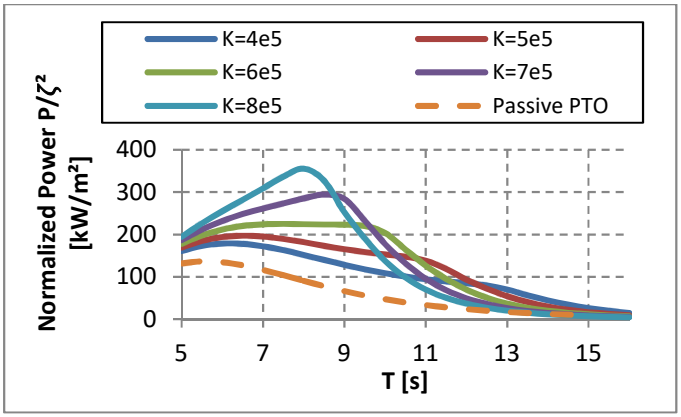

FIGURE 8- OPTIMIZED POWER FOR WEC B.

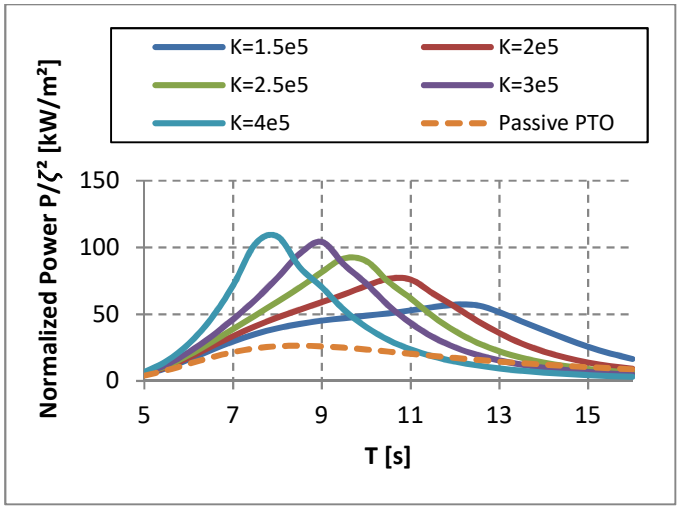

Figure 9- Optimized Power for WEC C.

Effects of PTO Strategies

Fig. 7, 8 and 9 show the results of the power absorption for passive and reactive PTOs on each WEC and some observations can be made from them. In the first place, as expected, the reactive PTO curves show much greater power capture than passive damping PTO curves. Varying the spring constant, the device can tune its resonance period in the incoming waves. This situation enhances the response amplitudes and therefore yields higher levels of power absorbed.

It is equally relevant to notice that when the device is tuned in lower periods of resonance the maximum power absorbed increases. Remembering the power absorption of the PTO given by equation 13, the effects of the velocity of oscillation are preponderant for a greater rate of absorption and lower periods of resonance induce in faster oscillations.

3.4.3. Optimized Response

The following study assesses the optimized response of each WEC operating at a sea state composed of regular waves. Each WEC is tuned in the resonance period $T = 8$ s according to the PTO parameters optimized in 3.4.2. and shown in table 2.

Table 2- PTO Parameters (optimized).

	K_{pto} [kN/m]	C_{pto} [kNs/m]
WEC A	600	75.1
WEC B	800	182.6
WEC C	400	65.5

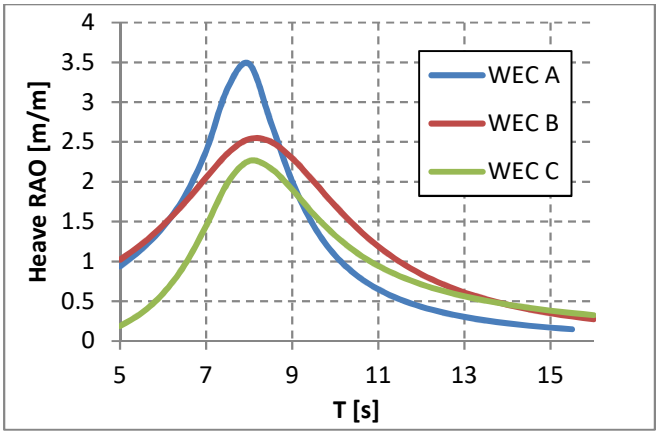

Figure 10- Heave Amplitudes (optimized).

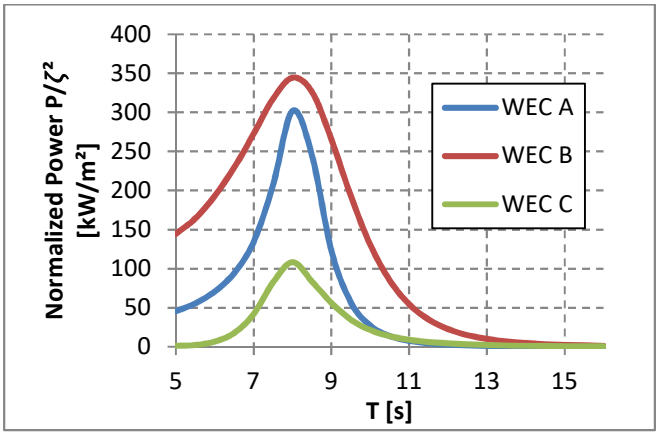

Figure 11- Power Absorption (optimized).

3.5. Discussions and Conclusion

Concerning the bandwidth, we note the WEC A exploits a narrower band of the sea state. Meaning that its capacity of energy absorption decays significantly after a short variance from its period of resonance. However, its higher amplitudes of oscillation on the resonance period (Fig. 10) reveal a good performance when this device is perfectly tuned in the peak period of the sea state. On the other hand, WEC B and WEC C own a broader bandwidth. We can relate this feature to the damping of each WEC since both own a damping superior to WEC A, namely radiation damping for WEC C and PTO damping for WEC B.

The excitation forces and inertial forces induce higher amplitudes of oscillation leading to higher levels of capture of wave energy since these forces enable a greater damping of the PTO. This statement is proved by the added mass and excitation force of WEC B and its great value of PTO damping. The excitation forces are specially expressive on the free surface as seen on the floater of WEC A and WEC B. Therefore, a fully submerged system like WEC C is subjected to much lesser excitation forces.

Is to be highlighted the significant difference between two-body systems and single-body systems concerning the maximum power absorbed. Tuning the two bodies in opposite phases maximizes the relative between each other and therefore the power absorption. The oscillations of WEC C are significantly smaller since this system is only composed of one oscillating body.

4. Response to Irregular Waves

It urges the need to study the performances of the WECs at wave climates with irregular waves since these conditions represent the real conditions faced by the systems on the sea.

4.1. Sea States

To compare the performance of each WEC, a set of sea states representative of the North Sea was considered [20]. Each sea state is defined by its significant wave height H_s and peak period T_p. The wave amplitude spectra is based on the parameterized JONSWAP spectrum.

Table 3- Reference sea states.

Sea State	H_s [m]	T_p [s]
1	0.75	5.45
2	1.25	5.98
3	1.75	6.59
4	2.25	7.22

4.2. Power Capture in Irregular Waves

In chapter 3, the optimization of the PTO was calculated by varying the parameters K and C in equation 13 to maximize the power absorption. However, this strategy does not apply in irregular waves since the maximum instantaneous power absorption does not necessarily means the maximum mean absorbed power. Hence, for this optimization, the wave spectrum must be taken into

consideration and therefore a new objective function is considered to maximize the power capture.

$$\bar{P} = C \int_0^{\infty} \omega_i^2 \left(\frac{X_{r,i}}{\zeta}\right)^2 S(\omega)\, d\omega \qquad (20)$$

As in chapter 3, the spring K is used for the reactive PTO.

4.2.1. Motion Constraints

Relative motion constraints are important for the practical design of WECs. The maximum stroke of the PTO is limited to its mechanism allowance. To prevent an excessive stroke length, one of the possible solution relies on the adjustment of the PTO force to constrain relative motion within the allowable range. However, this solution may reduce the power absorption. Another solution is to equip the device with end stoppers consisting in high stiffness springs at the end of the hydraulic cylinders of the PTO. In this solution, the power capture is not affected unless maximum stroke is reached, yet the continuous impact may damage its components. Hence, a trade-off between power capture and maximum allowable stroke must be studied.

For this study, each WEC is constrained to 3.5 m of amplitude.

Results

Once the WEC C presents significantly smaller dimensions, it might be meaningless the comparison between the other two devices. Therefore, it is reasonable the scaling of the model so it can match the dimensions of WEC A and WEC B. Considering the length of the reacting body WEC A and WEC B and the floater of WEC C, we have a scale factor $\alpha = 1.67$ which under Froude scaling, the power absorption scales $\alpha^{3.5}$. The WEC C* denotes the results contemplating the scaling factor α.

The results of power capture for the considered sea states are shown in table 4. The values obtained correspond to the optimized reactive PTO.

From this results, we can conclude some WECs are more suitable than other depending on the wave climate where they are deployed.

As seen before, the WEC A yields higher amplitudes of oscillation than the remaining systems which conduct to better results when it is tuned in the peak period of the spectrum as shown in sea states 1 and 2. However, in sea states 3 and 4, WEC B has revealed as the best option. This change is mainly due to the motion constraints since, in this sea states, the heights of the waves induce oscillations in the bodies beyond the allowed. Therefore, when the limit of the stroke is reached, the broader bandwidth of the WEC B permits a larger amount of energy absorption, hence this system is an adequate option for more energetic waves.

The WEC C improves its performance with higher waves, decreasing its differences to the other systems. Being a single-body system, the WEC C needs a more energetic wave to achieve significant heave amplitudes where its broad bandwidth also contributes to higher levels of absorption.

4.3. Case Study in Madeira Archipelago

It is also meaningful the study of long-term sea states as a succession of short-term sea states. In the present study, two scatter diagrams were chosen from two different locations in Madeira Islands [21]. This archipelago lies in the North Atlantic Ocean about 1000km from the Continent. Due to its geographical position, Madeira Islands own a vast field of powerful wave surrounding them making this, a suitable place for wave energy conversion. The plotted scatter diagrams subjected to study are referring to near-shore sites in Madeira (MA1) and Porto Santo (PS1), the two main islands of the Archipelago. These two particularly sites were chosen due to their differences concerning the width of their wave spectrum. While MA1 shows a wider range of waves, the PS1 reveals a smaller variance of the waves heights, yet more powerful.

The scatter diagrams as shown in table 5 and 6 are the result of statistical analysis and were generated using data from the time interval of 07/10/1997-01/03/1998 and 01/12/2000-05/03/2001 and wave period time

sequences resulting from simulations with the SWAN model. The sea states are structured into bin of 0.5 s × 0.5 m $(\Delta T_p \times \Delta H_s)$ where each bin is expressed in percentage the probability of occurrence the respective sea state.

Results

The results obtained in table 7 and 8 are the outcome of an optimization of each PTO considering the probability of occurrence of each spectrum.

Although MA1 and PS1 have different depths, 50 m and 40 m respectively, it was considered the 40 m depths in both sites. This approach is convenient to compare the WECs performance subjected only to different wave climates without any differences regarding the wave dispersion. Since WEC C is bottom fixed, this assumption is especially significant for its results, for this reason, a sensitivity test of WEC C performance to depth variance is executed in chapter 4.3.2 where it includes the real depth of MA1.

Table 4- Results of Reference Sea States.

	Sea States							
	1		2		3		4	
	$\bar{P}$ [kW]	Dif [%]	$\bar{P}$ [kW]	Dif [%]	$\bar{P}$ [kW]	Dif [%]	$\bar{P}$ [kW]	Dif [%]
WEC A	2.1		32.5		119.4		193.1	
WEC B	1.8	-13.8	27.3	-16.2	142.8	19.6	245.9	27.3
WEC C	0.3	-83.2	4.7	-85.6	25.1	-78.9	89.5	-53.7
WEC C*	2.1	1.0	28.0	-13.9	150.8	26.3	537.0	178.0

Table 5- Scatter Diagram MA1.

	Tp (s)																
Hs (m)	5	5.5	6	6.5	7	7.5	8	8.5	9	9.5	10	10.5	11	11.5	12	12.5	13
0.5	0	0	0	0	0.1	1.2	0.05	0	0	0	0	0	0	0	0	0	0
1	0	0	0	0.3	0.1	1.4	0.55	1.05	1	0.3	0.2	0.05	0.05	0	0	0	0
1.5	0	0.1	0.5	0.1	0.4	0.8	2.51	1.05	1.5	1.6	1.6	2.26	0.55	0.55	0.05	0.26	0
2	0	0.5	0.8	1.4	0.4	0.3	1.76	1	0.8	0.8	2.01	3.56	2.76	2.27	1.05	0.55	0.2
2.5	0	0	0	1.5	0.9	1.81	0.5	1.05	0.9	1.3	1.3	1.26	1.5	2.27	1.76	0.76	0.55
3	0	0	0	0.2	0.8	0.1	0.3	0.55	0.4	0.5	0.5	0.76	0.05	0.76	1.76	1.05	0.65
3.5	0	0	0	0	0	0.2	0.55	0.1	0.5	0.6	0.2	0.27	0.05	0.27	0.76	0.76	0.76
4	0	0	0	0	0	0.6	0.55	0.3	0.3	0.2	0.1	0.05	0.05	0.27	0.55	0.26	0.76
4.5	0	0	0	0	0	0.1	0.3	0.5	0.4	0.1	0.2	0.05	0	0	0	0.05	0.1
5	0	0	0	0	0	0	0	0	0.1	0.3	0	0.05	0.05	0.05	0.05	0	0.1
5.5	0	0	0	0	0	0	0	0.05	0.1	0.1	0	0	0	0	0.05	0.05	0.1
6	0	0	0	0	0	0	0	0	0	0.2	0.1	0	0.05	0	0.3	0.05	0.05
6.5	0	0	0	0	0	0	0	0	0	0	0.1	0.05	0	0.05	0.05	0.05	0.05
7	0	0	0	0	0	0	0	0	0	0	0.1	0.05	0	0	0	0	0
7.5	0	0	0	0	0	0	0	0	0	0	0	0	0	0	0.05	0	0
8	0	0	0	0	0	0	0	0	0	0	0	0	0	0	0.05	0	0

Table 6- Scatter Diagram PS1.

	Tp (s)																
Hs (m)	5	5.5	6	6.5	7	7.5	8	8.5	9	9.5	10	10.5	11	11.5	12	12.5	13
0.5	0	0	0	0	0.1	0.1	0	0	0	0	0	0	0	0	0	0	0
1	0	0	0	0.1	1.4	0.4	0.52	0.26	0.08	0.05	0	0	0	0	0	0	0
1.5	0	0	0	0.1	2.01	0.6	1.76	0.76	1.26	1.52	0.76	0.52	0.5	0	0	0	0.05
2	0	0	0	0.1	0.7	2.21	2.26	1	2.26	2.01	2.52	2.52	2.26	1.2	0.56	0.08	0
2.5	0	0	0	0	0	0.1	0.76	0.76	1.76	0.52	1.52	2.01	3.05	3.41	1.56	1.26	0.08
3	0	0	0	0	0	0	0	0.52	0.52	1.05	0.3	0.3	1.05	3.11	2.76	2.56	0.76
3.5	0	0	0	0	0	0	0	0.05	0.26	0.26	0.52	0.3	0.76	0.7	1.5	1.56	0.76
4	0	0	0	0	0	0	0	0	0	0.08	0.5	0.26	0.26	0	0.26	0.56	0.56
4.5	0	0	0	0	0	0	0	0	0	0	0.26	0	0.05	0.4	0.05	0.05	0.76
5	0	0	0	0	0	0	0	0	0	0	0	0.05	0	0	0.05	0.05	0.05
5.5	0	0	0	0	0	0	0	0	0	0	0	0	0.05	0.2	0.05	0.05	0.05
6	0	0	0	0	0	0	0	0	0	0	0	0	0	0	0.08	0.05	0.26
6.5	0	0	0	0	0	0	0	0	0	0	0	0	0	0	0	0.05	0
7	0	0	0	0	0	0	0	0	0	0	0	0	0	0	0.08	0.05	0
7.5	0	0	0	0	0	0	0	0	0	0	0	0	0	0	0	0	0.05
8	0	0	0	0	0	0	0	0	0	0	0	0	0	0	0	0	0

Table 7- Mean Power Absorbed MA1.

	MA1		
	$\overline{P}$ [kW]	C_{pto} [kNs/m]	K_{pto} [kN/m]
WEC A	57.0	81.3	500
WEC B	86.1	132.9	750
WEC C	40.0	61.4	250

Table 8- Mean Power Absorbed PS1.

	PS1		
	$\overline{P}$ [kW]	C_{pto} [kNs/m]	K_{pto} [kN/m]
WEC A	51.1	67.7	400
WEC B	80.6	115.6	650
WEC C	50.3	57.0	170

The WEC B has revealed the best performance at both locations. The combination of a broad bandwidth, large PTO damping and moderate oscillating amplitudes gives to this device the capacity to exploit larger amounts of energy on these wave climates.

On the other hand, the WEC A is significantly affected by the motion constraints since this system reaches the limits of absorption with waves of moderate heights. Moreover, its narrow bandwidth reduces the range of periods with significant energy absorption.

The low heave amplitudes of WEC C permit its tuning in the most powerful regime of the diagram without being affected by the motion constraints. Making use of its broad bandwidth, this system exploits a wide range of energetic waves, revealing results close to the other two WECs.

Although the most energetic regime at PS1, the performance of the WEC A and WEC B have worsened. There are two possible explanations for this situation. First, due to the higher occurrence of greater waves, the limits of the amplitudes of oscillation are reached more often. Second, the average period of PS1 is superior to MA1, from equation 13, the power absorption is greater in shorter periods of oscillation, therefore at this location the levels of power absorption are inferior to MA1.

4.3.1. Sensitivity Study of WEC Performance to Viscous Resistance

Once the drag coefficients employed in the calculation are obtained from the literature for the WEC A and B and estimated for the WEC C, it is found relevant the

sensitivity study to acquire insight into this uncertainty in WEC performance.

The power performance analysis at the Madeira Archipelago was re-executed for each WEC with the drag coefficients values of 50% and 150% of the coefficients values used for the previous studies.

The results are summarized in tables 9,10 and 11.

Table 9- Results of Sensitivity Study to Drag Coefficient for WEC A.

	MA1		PS1	
C_d	$\overline{P}$ [kW]	Dif [%]	$\overline{P}$ [kW]	Dif [%]
1.9	57.0	Base	51.1	Base
0.95	74.0	29.8	72.2	41.3
2.85	47.0	-17.5	38.1	-25.5

Table 10- Results of Sensitivity Study to Drag Coefficient for WEC B.

	MA1		PS1	
C_d	$\overline{P}$ [kW]	Dif [%]	$\overline{P}$ [kW]	Dif [%]
2.8	86.2	Base	80.6	Base
1.4	120.0	39.2	125.5	55.7
4.2	67.5	-21.7	58.8	-27.0

Table 11- Results of Sensitivity Study to Drag Coefficient for WEC C.

	MA1		PS1	
C_d	$\overline{P}$ [kW]	Dif [%]	$\overline{P}$ [kW]	Dif [%]
0.83	40.1	Base	49.0	Base
0.42	60.8	51.6	66.7	36.0
1.25	28.8	-28.2	36.3	-26.0

Table 12- Average Results of Sensitivity Study to Drag Coefficient [%].

0.5 C_d		1.5 C_d	
MA1	**PS1**	**MA1**	**PS1**
40.2	46.6	-22.4	-27.5

4.3.2. Sensitivity Study of WEC Performance to Design Parameters

As mentioned before, each WEC has distinct features concerning their design and as result of those differences, each WEC behaves differently to the excitation of the wave. For this reason, a new sensitivity study was performed for each WEC where relevant design variables are changed. For this study is considered again the scatter diagrams of Madeira Islands.

The WEC A features a water ballast tank as the reacting body being the mass of this device the main characteristic of differentiation to the others. Therefore, is carried out a sensitivity test to the variance of its mass for values of 90%, 110% and 120% of the original mass.

Table 13- Results of Sensitivity Study to Design Parameters for WEC A.

	MA1		PS1	
	$\overline{P}$ [kW]	Dif [%]	$\overline{P}$ [kW]	Dif [%]
m_2	57.0	Base	51.1	Base
$0.9m_2$	45.5	-20.3	36.5	-28.5
$1.1m_2$	69.3	21.5	68.2	33.5
$1.2m_2$	82.3	44.2	87.8	71.7

The WEC B features a large heave plate to increase its radiation forces, for this reason, it is performed a sensitivity test for the plate diameter variance. A set of plates with 90%, 110% and 120% of the original diameter were used in the realization of the study.

Table 14- Results of Sensitivity Study to Design Parameters for WEC B.

	MA1		PS1	
	$\overline{P}$ [kW]	Dif [%]	$\overline{P}$ [kW]	Dif [%]
D	86.2	Base	75.6	Base
0.9D	59.8	-30.6	47.7	-36.9
1.1D	114.7	33.1	110.2	45.7
1.2D	152.3	76.7	155.3	105.3

Unlike the WEC A and WEC B, the WEC C is totally submerged. Therefore, the effects of the dispersion due

to depth shall be studied. In this study, the result of MA1 for a depth $h = 50$ m is particularly important since it shows the power absorption for the real depth of this site.

Table 15- Results of Sensitivity Study to Design Parameters for WEC C.

	MA1		PS1	
h [m]	$\overline{P}$ [kW]	Dif [%]	$\overline{P}$ [kW]	Dif [%]
40	40.1	Base	49.0	Base
35	64.4	60.7	69.4	41.6
45	24.8	-38.2	34.6	-29.5
50	16.3	-59.3	22.4	-55.4

4.3.3. Sensitivity Study of WEC Performance to Motion Constraints

The power absorbed by the WEC is determined by the oscillation amplitude of its bodies. However, due to the restrictions of the PTO, those amplitudes are limited to a certain interval to ensure the integrity of the equipment. For this sensitivity study, the maximum allowable amplitude for the WECs varies between 3 m and 4.5 m. The results are shown in tables 16, 17 and 18

Table 16- Results of Sensitivity Study to Motion Constraints for WEC A.

	MA1		PS1	
	$\overline{P}$ [kW]	Dif [%]	$\overline{P}$ [kW]	Dif [%]
3.5	57.0	Base	51.1	Base
3	52.5	-8.0	48.1	-6.0
4	61.7	8.1	53.3	4.3
4.5	65.2	14.3	54.8	7.2

Table 17- Results of Sensitivity Study to Motion Constraints for WEC B.

	MA1		PS1	
	$\overline{P}$ [kW]	Dif [%]	$\overline{P}$ [kW]	Dif [%]
3.5	86.2	Base	80.6	Base
3	80.6	-6.5	77.6	-3.7
4	90.3	4.8	82.4	2.2
4.5	93.5	8.5	83.3	3.4

Table 18- Results of Sensitivity Study to Motion Constraints for WEC C.

	MA1		PS1	
	$\overline{P}$ [kW]	Dif [%]	$\overline{P}$ [kW]	Dif [%]
3.5	40.1	Base	50.4	Base
3	37.8	-5.6	46.5	-7.7
4	41.8	4.2	53.3	5.9
4.5	43.3	8.1	55.3	9.8

Table 19- Average Results of Sensitivity Study to Motion Constraint [%].

3		4		4.5	
MA1	**PS1**	**MA1**	**PS1**	**MA1**	**PS1**
-6.7	-5.8	5.7	4.1	10.3	6.8

4.4. Discussions and Conclusions

After the present study of the WEC responses to irregular waves, some conclusions can be drawn.

The streamlined reacting body of WEC A is suitable for sea states with small significant wave heights as result of its high oscillating amplitudes. However, is considerably affected by the motion constraints on a more powerful regime. Due to its narrow bandwidth, this system is adequate to spectra with low amplitude variance. Increasing the mass of its reacting body enhances the performance of this device.

The system B with a heave plate has revealed good performances at several wave climates with special prevalence for more energetic waves due to its broad bandwidth, large damping of the PTO and moderate heave amplitudes. The power absorption can be greatly increased by scaling the diameter of its heave plate. Increasing 20% its diameter results in 2 times higher amount of energy captured.

The WEC C, due to its single-body system is mostly suitable for very energetic sea states. With a broad bandwidth and low heave amplitudes, this device is capable of tuning in very energetic regimes without significant effects of the motion constraints. However, it

is very sensitive to the depth of the location where is deployed, not being viable for depth greater than 40 m.

All systems are very sensitives to the employed value of the drag coefficient while the effect of motion constraints on each WEC varies, being more significant on the WECs with higher amplitudes or tuned in more energetic periods.

References

[1] S. Hellas, "Wave Energy." [Online]. Available: http://www.sigmahellas.gr.

[2] J. Cruz, *Ocean Wave Energy*. 2008.

[3] A. F. de O. Falcão, "Wave energy utilization: A review of the technologies," *Renewable and Sustainable Energy Reviews*, vol. 14, no. 3. pp. 899–918, 2010.

[4] J. Zumerchik and S. L. Danver, *Seas and Waterways of the World*. 2010.

[5] M. E. McCormick, *Ocean Wave Energy Conversion*, vol. 45. 1981.

[6] T. Setoguchi and M. Takao, "Current status of self rectifying air turbines for wave energy conversion," *Energy Convers. Manag.*, vol. 47, no. 15–16, pp. 2382–2396, 2006.

[7] H. Hotta, T. Miyazaki, Y. Washio, and S. I. Ishii, "On the performance of the wave power device Kaimei - the results on the open sea tests.," *IN: OMAE 1988 HOUSTON, PROC. SEVENTH INT. CONF. ON OFFSHORE MECHANICS AND ARCTIC ENGINEERING, (HOUSTON, U.S.A.: FEB. 7-12, 19*, vol. I, New Yor. pp. 91–96, 1988.

[8] C. Grove-Palmer, "Wave energy in the United Kingdom: a review of the programme June 1975 to March 1982.," pp. 23–54, 1982.

[9] A. F. O. Falcão, "Modelling of Wave Energy Conversion," pp. 1–38, 2014.

[10] J. Falnes and M. Perlin, *Ocean Waves and Oscillating Systems: Linear Interactions Including Wave-Energy Extraction*, vol. 56, no. 1. 2003.

[11] I. G. Morrison, "Oscillating Water Column Modelling," *Proc. 23rd Conf. Coast. Eng. Venice, Italy, 1992.*, pp. 502–511, 1992.

[12] M. J. Muliawan, Z. Gao, T. Moan, and A. Babarit, "Analysis of a Two-Body Floating Wave Energy Converter With Particular Focus on the Effects of Power Take-Off and Mooring Systems on Energy Capture Analysis of a Two-Body Floating Wave Energy Converter With Particular Focus on the Effects of Power Take-Off," 2013.

[13] J. Weber, F. Mouwen, a. Parish, and D. Robertson, "Wavebob – Research & Development Network and Tools in the Context of Systems Engineering," *Ewtec*, no. Proc. of the 8th European Wave and Tidal Energy Conf., Uppsala, Sweden, pp. 416–420, 2009.

[14] F. Mouwen, "Presentation on Wavebob to Engineers Ireland," 2008.

[15] O. P. Technologies, "No Title." [Online]. Available: www.oceanpowertechnologies.com.

[16] M. Mekhiche and K. A. Edwards, "OCEAN POWER TECHNOLOGIES POWERBUOY ®: SYSTEM - LEVEL DESIGN , DEVELOPMENT AND VALIDATION METHODOLOGY," pp. 1–9, 2014.

[17] K. Edwards, J. Bretl, and J. Montgomery, "Comparison of Model and Measured Power from a WEC Ocean Deployment Background : OPT PowerBuoy ®," 2015.

[18] M. G. Prado, F. Gardner, M. Damen, and H. Polinder, "Modelling and test results of the Archimedes wave swing Modelling and test results of the Archimedes wave swing."

[19] M. Prado and H. Polinder, *Case study of the Archimedes Wave Swing (AWS) direct drive wave energy pilot plant*. Woodhead Publishing Limited.

[20] Y. Goda, *Random seas and design of maritime structures*, vol. 15. 2000.

[21] E. Rusu and C. G. Soares, "Wave energy pattern around the Madeira Islands Wave energy pattern around the Madeira Islands," no. September, 2012.